

Adapted Human Pose: Monocular 3D Human Pose Estimation with Zero Real 3D Pose Data

Shuangjun Liu · Naveen Sehgal · Sarah Ostadabbas

Received: date / Accepted: date

Abstract The ultimate goal for an inference model is to be robust and functional in real life applications. However, training vs. test data domain gaps often negatively affect model performance. This issue is especially critical for the monocular 3D human pose estimation problem, in which 3D human data is often collected in a controlled lab setting. In this paper, we focus on alleviating the negative effect of domain shift by presenting our adapted human pose (AHuP) approach that addresses adaptation problems in both appearance and pose spaces. AHuP is built around a practical assumption that in real applications, data from target domain could be inaccessible or only limited information can be acquired. We illustrate the 3D pose estimation performance of AHuP in two scenarios. First, when source and target data differ significantly in both appearance and pose spaces, in which we learn from synthetic 3D human data (with zero real 3D human data) and show comparable performance with the state-of-the-art 3D pose estimation models that have full access to the real 3D human pose benchmarks for training. Second, when source and target datasets differ mainly in the pose space, in which AHuP approach can be applied to further improve the performance of the state-of-the-art models when tested on the datasets different from their training dataset.

Keywords 3D human pose estimation · domain shift · semantic aware adaptation · synthetic human datasets.

1 Introduction

With the great endeavor of the computer vision community, significant advancements have been achieved for 3D

human pose estimation with ever improving performance on well recognized benchmarks [19]. Existing approaches come from versatile genres such as end-to-end learning [25], direct 2D-to-3D lifting [35] and even unsupervised methods [8]. Although improved performance has been reported with decreased information dependence on the training sets [35,8], the majority of these studies are conducted via a training/testing data split from the same benchmark datasets, which share very similar contexts. In essence, these 3D human pose benchmarks could be quite different from the real life applications, and the domain gap between the source data and target applications could lead to potential performance drops. And, while domain shift issue has been extensively investigated for the classification tasks [12,58], it has been rarely addressed in the pose regression problems.

In this paper, we investigate how domain shift influences the 3D pose estimation model performance and more importantly how to counter its adverse effect. Our approach incorporates a semantically aware adaptation technique as well as a skeletal pose adaptation method towards developing a robust 3D human pose estimation model. Our approach is not only capable of training monocular 3D human pose estimation model using zero real 3D human pose data, but also can be added to the existing state-of-the-art (SOTA) models as a light weighted head for adaptation when tested under a novel context or dataset.

Unfortunately, performance evaluation of the 3D pose estimation models under real world applications is not widely conducted, since acquiring labeled 3D human pose data often requires professional motion capture systems [19] and a few available datasets are collected under lab settings with very limited samples in the wild [37]. This issue could inherently result in the similarity of the environments, the camera settings (in both extrinsic and intrinsic parameters), and also human pose distributions between training and evaluation data splits. As a consequence, training and

S. Liu, N. Sehgal, and S. Ostadabbas
Augmented Cognition Lab, Electrical and Computer Engineering Department, Northeastern University. E-mail: shuliu@ece.neu.edu, sehgal.n@husky.neu.edu, ostadabbas@ece.neu.edu

testing on the same benchmark disproportionately take advantage from these context similarities, which does not always hold in a practical application. For 2D-to-3D lifting approach [35], such mapping is conducted inherently under a fixed camera setting. The model in [8] although employs no 3D pose data directly, its 2D pose data is a direct projection of the 3D data from the same benchmark, which holds identical pose semantics and distributions of their target domain. It is also evident in their reported performance that using pose data without adaptation leads to significant performance drop. Even for template-based pose estimation approaches such as [4], the template is explicitly adapted to the poses from the target domain using the motion and shape (Mosh) capture approach from sparse markers [31]. Please note that in these approaches, to adapt the pose, the real 3D human benchmark data has to be employed in Mosh approach [31]. In the recent work [26], few training 3D human training data can be extensively augmented for training and impressive result has been achieved. Yet the focus is on augmentation where the real 3D human data though little are still needed.

Admittedly, it is a good practice to employ as much information as we can get for an improved performance. Yet, in a real life application, we may have access to no pose or image data in the target domain, or at best only limited number of measurements can be collected from the target domain apriori.

Here, we introduce our adapted human pose (AHuP) approach, which allows us to study the monocular 3D human pose estimation problem under a highly unaware context assuming zero or very limited amount of information from the target domain. On one hand, we use synthetic human simulation as an efficient and easy-to-produce source pose data generator, which leads to a training set which is very different from the target real 3D pose benchmarks. With synthetic appearances, simplified skeletons, and different pose distribution, learning from synthetic human and testing on real 3D human poses becomes a typical manifestation of the potential domain shift. Although, introducing synthetic data for learning is not a new idea, yet competitive performance is only reported by further incorporating real 3D human data into the current models [61]. Furthermore, there is no specific discussion on how these differences affect the pose estimation performance and what is the proper way towards addressing the challenges associated with the domain gap caused by training vs. testing data distributions. On the other hand, for the existing SOTA 3D human pose estimation models, AHuP can be also added as a light weighted adaptation head for performance improvement when a novel context or dataset is used during the test phase. This improvement is observed on several SOTA models and on all training and testing combinations in our study. In short, our work makes the following contributions:

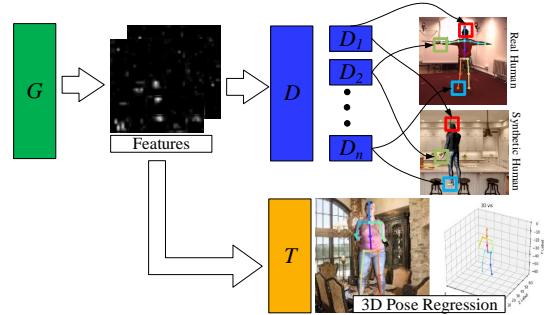


Fig. 1: The proposed adapted human pose (AHuP) framework and our semantically aware adaptation (SAA) approach for 3D human pose estimation. G stands for the feature extractor, T for task head, D for discriminator and D_i stands for the i -th channel of D .

- Presents adapted human pose (AHuP) approach (see Fig. 1) that improves the performance of the state-of-the-art 3D human pose estimation models for both synthetic to real and real to real cases when training and test data come from different contexts. One of our adapted synthetic model by using zero real 3D human pose data shows comparable performance with the SOTA pose estimation models trained based on a large amount of real 3D human pose data.
- Proposes a semantically aware adaptation (SAA) method to enhance the cross-domain feature space adaptation, which shows noticeable pose estimation performance improvement over conventional domain adaptation techniques.
- Introduces a skeletal pose adaptation (SPA) approach, which takes only limited amount of information from the target domain to adapt the pose, instead of requiring the whole 3D pose data from the target dataset for adaptation purpose.
- Demonstrates the effect of our proposed AHuP approach, quantitatively and qualitatively by visualizations in both pose space and feature space.
- Introduces and publicly releases a new 3D scan-based synthetic human dataset called ScanAva+, which is an extended version of our previous ScanAVA dataset (which only had 15 scans), by adding 26 new synthetic human objects with higher texture and size variations.

2 Related work

In this section, we provide an overview of the state-of-the-art in the field of 3D human pose estimation and related works that leverage synthetic human models to deal with the 3D data scarcity issues. We also give a summary of the works that employ domain adaptation techniques to close the gap

between their training and the test datasets, especially when synthetic data are employed.

2.1 The Problem of Monocular 3D Human Pose Estimation

For monocular 3D human pose estimation, early attempts followed the 2D pose paradigm and conducted straightforward end-to-end training directly on available 3D human pose datasets such as Human 3.6M [19] and HumanEva [53]. However, the resultant models are often not very generalizable, especially when applied on real world (“in the wild”) images. This is mainly due to the fact that most 3D human datasets are collected under controlled lab settings that lack meaningful variations. To improve the generalization ability in the wild, another line of work takes a two-stage strategy, where it first trains a known 2D pose estimation model [42], then recovers the 3D poses on top of that [69]. Some recent works further mix 2D and 3D pose data together to solve the pose estimation problem.

In [46], authors considered 3D pose a multi-task learning process using 2D pose and depth data. [68] further incorporated a weakly-supervised loss in order to integrate 2D and 3D data. The 3D pose estimation is also solved in a 2D-to-3D lifting manner without learning from the corresponding image or even in an unsupervised manner [8]. Template based approach has also been employed by fitting the projected silhouette with prior constraints [4]. In recent works, kinematic constraints have also been introduced where human motion sequence data is required [64,43]

Another approach in 3D pose estimation is to employ synthetic human pose data, summarized in the following section. In short, no matter what exact methodology is used, methods with competitive performance in 3D human pose estimation field usually cannot avoid employing some real 3D human pose data in their training process, which makes them expensive to train. Even though the very recent works in [23,50,20] successfully estimate 3D poses without any explicit 3D labels, they use multi-view setting in which 3D coordinates under that can be estimated from the 2D pose via the multi-view geometry. However, a calibrated multi-view setting will not be always available in many applications.

2.2 Synthetic Human Pose Data

Employing synthetic data to solve real world problems is not a new concept in the computer vision field. For low level vision tasks, synthetic images have been employed for stereo vision [45] and optical flow estimation [5]. For higher level tasks, computer-aided design (CAD) models have also been extensively used for object detection [27,44,34] or segmentation [18].

Synthetic human figures have been extensively used for learning purposes, such as silhouette-based action recognition tasks [48], and crowd counting [63]. Towards the human pose estimation, [61], SURREAL provides 145 subjects and over 6.5 million frames with detailed pose and segmentation labels based on a morphable human template. Templates from the shape completion and animation of people (SCAPE) [3] have also been employed for large-scale 3D human pose dataset forming [9]. Another branch is synthesizing human pose data directly via a human body scanning process, which could be limiting in terms of the number of scans, yet garment geometry details are better preserved, such as our recently developed Scanned Avatar (ScanAva+) dataset that contains 3D scans of 41 human subjects [29]. Nonetheless, no matter how realistic the simulated data looks and despite applying conventional domain adaptation methods on them, models trained on the synthetic data alone perform noticeable worse than models trained on real human pose data [9].

2.3 Synthetic vs. Real Data Domain Adaptation

Domain adaptation is a long standing topic in the computer vision field, yet synthetic to real data domain adaptation for task transfer learning still remains a challenge. Well-known algorithms mainly address the domain gap issue at the feature level by aligning extracted features from both domains and subsequently minimizing certain distance measures between them, such as maximum mean discrepancy [30], correlation distance [54], or adversarial discrimination loss [12,58]. However, such measures usually do not guarantee semantic consistency. Though this issue has been addressed recently [32], yet usually stays in the classification problems but not for pose regression. On the other hand, pixel level adaptation pursues visual plausibility [21,72], which can be deemed as a style transfer approach. However, their performance for inference tasks have not been studied. Authors in [17] combined cycle consistency with domain adaptation in both pixel and feature levels and reported an improvement in the synthetic data based segmentation tasks. In many adaptation techniques, adversary learning is a major component to reduce cross-domain discrepancies [60], however the adaptation for regression tasks have not been extensively studied.

Another important concept during adaptation is the semantic consistency, whose absence is a critical cause of performance degradation [32]. In the image synthesis approach described in [62], the authors enforce semantic consistency with an L_1 loss. The loss is computed per-layer between features extracted from a synthetic image and a real sampled image using a pre-trained VGG model, with an adaptive weight that decreases for deeper layers. In [6], for unsupervised domain adaptation, the authors use a two-stream

convolutional neural network (CNN), one for the source domain and one for the target domain, with shared weights. When training a classifier, they assign pseudo-labels and then use an adaptive centroid alignment to offset the negative influence from false pseudo labels and enforce cross-domain class consistency. Similarly in the segmentation task of [32], the authors propose a category-level adversarial network, where two classifiers identify classes whose features are distributed differently between the source and target domains and proportionally increase an adversarial loss to enforce semantic alignment across domains.

Despite being an important concept, semantic consistency is not typically used in approaches for pose regression. More commonly, it is used for classification tasks such as in [32, 41], and also for image synthesis purposes [62]. Though adversarial learning is introduced in human pose estimation before [65], however it is mainly used for pose regularization purpose, where the training portion of the benchmark dataset is required.

In this work, we explore how 3D pose estimation performance will be negatively affected by the domain shift between source and target domains through the use of synthetic 3D human pose data as our training source. More importantly, we present the AHuP approach which incorporates our counter action adaptation techniques in both feature space and pose space.

3 Introducing Adapted Human Pose (AHuP)

When a pre-trained 3D human pose estimation model is employed in a real world application, many context elements are different from the benchmark that the model was trained on: the person will no longer wear tight clothes to facilitate the motion capture process, no tracker bead is attached, the background will be more versatile compared to a lab environment, and a different pose semantic definition may be used. As in most cases, human pose is estimated based on extracted image patches [68, 39], so we can assume the differences mainly come from the appearance and pose semantics.

To investigate the effect of these differences, we design our adapted human pose (AHuP) model to learn from a source data with noticeable differences in both appearance and pose distributions compared to the common 3D pose benchmarks. An overview of our AHuP framework is shown in Fig. 1. In our primary study, we choose synthetic human pose data as our model training source since they hold visible unrealistic appearances with simplified skeletons, and their simulated poses although similar will never be the same as a real human. Furthermore, synthetic 3D human pose data and label pairing can be acquired more easily, which means using them as a source data is a relatively

cheaper solution. In our secondary study, when both training and test data are from real humans, adding AHuP as a light weight head to the pre-trained SOTA 3D pose estimation model demonstrates universal effectiveness in estimation accuracy improvements, especially models are applied to a new context/dataset.

3.1 Semantic Aware Adaptation (SAA)

Domain shift is an common issue when a model learned from domain A is applied in domain B for a similar task. There are consistent efforts in the computer vision community to address such issue. For discriminative tasks [59], despite variations in the specifics of the model components [17, 58], a commonly employed structure is to adapt two datasets A and B for a common task network T , by forming a feature extractor network G (or two for an asymmetric mapping case). This will map two datasets into a common feature space by minimizing a distance measure, such as the maximum mean discrepancy [47], or by confusing the discriminator with a generative adversarial network (GAN) structure [59]. Such distance measures are usually based on the statistics of overall feature maps [59] or local patches [21], uniformly. Although related studies are mainly conducted for classification tasks, there are also recent works that begin to address the segmentation problems with cycle consistency [17].

However, one problem often overlooked is the semantic meaning consistency between two datasets, which so far has been limited to the classification problems [32]. If the same semantic entity demonstrates varying patterns in different domains, it is very possible that in an image/feature space, the nearest neighbors from two domains do not hold the same semantic meaning. A common solution to shorten the overall distance between domains is aligning nearest neighbored patterns together to blur their domain identities. However, what if the well-aligned pattern comes out to hold different semantic meanings as Fig. 2a displays? Such adaptation will possibly turn out to make the result even more misleading, especially for the regression tasks such as human pose estimation, where body parts are usually more similar than distinct categories in a classification task.

We argue that the adaptation process should emphasize the semantic awareness in distance measures to achieve a semantically aware adaptation (SAA).

In AHuP, an intuitive way to achieve SAA is employing individual discriminator for each recognizable body parts. For efficiency, we use a multi-channel structure for AHuP to indicate different body parts as shown in Fig. 1, where D stands for the discriminator, D_i stands for the i -th channel of the discriminator for corresponding joint, G stands for the feature extractor and T stands for the task head as the

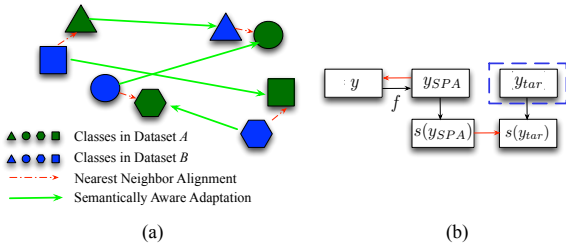


Fig. 2: (a) Semantically aware adaptation (SAA) vs. nearest neighbor alignment between datasets A and B , assumed to be from two different domains. (b) Skeletal pose adaptation (SPA) based on dual direction pivoting to both source and target in different representation. Black arrow indicates the forward mapping. Red arrow indicates the pivoting direction.

3D pose regression. As the extracted features from the backbone network G suppose to be highly generalized into a low resolution, inspired by patchGAN [21], we design the discriminator D to be feature-wise by setting the convolution kernel size to one with logistic regression. During training process, for each channel, only the corresponding feature will be activated based on the joint location. We avoid using any 3D human pose benchmark in this process by learning this information from the available 2D human datasets.

We employ the adversarial learning strategy by training D , G , and T networks, iteratively in an adversarial manner. For each input image x , we add a domain indicator $d(x)$ as 0 or 1 to indicate if it is real or synthetic, respectively. During D phase, we optimize D by minimizing the SAA_D loss as:

$$L_{SAA_D} = - \sum_{i=1}^N \mathbb{1}(c = J_{hm}(i)) (d(x) \log D_i(G(x))[c] + (1 - d(x)) \log (1 - D_i(G(x))[c]),) \quad (1)$$

where, N is the total joint numbers, c stands for the coordinate in the feature space, $D_i(\cdot)[c]$ stands for the i -th channel of D at coordinate c , $J_{hm}(i)$ is the i -th joint location in heatmap space. Compared to the conventional adaptation approaches [54, 58, 59], where the feature adaptation is over the whole image region, our approach specifies the semantic meaning via multi-channel discriminator.

We train the G and T networks together by minimize the regression error and confusing the D at the same time. We employ the cross entropy loss between the D prediction and a uniform distribution for confusing purpose as:

$$L_{conf} = - \sum_{i=1}^N \mathbb{1}(c = J_{hm}(i)) \left(\frac{1}{2} \log D_i(G(x))[c] \right). \quad (2)$$

The total loss during G and T phase is given as:

$$L_{SAA_{GT}} = \|y_{gt} - T(G(y))\|_1 + \lambda L_{conf}, \quad (3)$$

where λ is the coefficient for confusion loss, y_{gt} is the pose ground truth, and we use norm L_1 for regression supervision.

3.2 Skeletal Pose Adaptation (SPA)

Pose adaptation has been extensively employed in many of the 3D human pose estimation works, especially when data outside of the benchmark domains are introduced. The main idea is to align the introduced pose or its 2D projection ([8]) with the target domain either by direct mapping [4] or via a discriminator to detect fake poses [65]. The underlying assumption here is that there is an extensively collected target pose data to be aligned to which is not usually the case in real application. Instead, it is more reasonable to assume that only some countable low dimensional and interpretable parameters from the target domain could be gathered, such as the tailor measurements of the body limbs.

In order to achieve the skeletal pose adaptation (SPA), we use the normalized limb length vector $s(y)$ as the skeletal descriptor with the shoulder width as its normalization factor. Due to the different pose semantic definition and subjects' physiques, this descriptor could vary among different datasets. The aligned pose is given as $y_{SPA} = y + f(y)$, where y is the output of the pose estimation network as $y = T(G(x))$ in Fig. 1, f is a mapping function which is a multi-layer regression network in our design. What we want from this mapping is a pose holding similar semantic meaning with the source domain and at the same time a skeleton similar to the target domain. So, we employ a dual direction pivoting strategy in both pose and skeleton spaces by pushing the mapped pose to the source pose and at the same time pushing the mapped skeleton to the target skeleton, as shown in Fig. 2b.

To be specific, in original pose representation, by pivoting the resultant pose back to its original pose estimation y , we assume the mapped pose should not be far away from the source, namely the original pose prediction to keep the pose semantic meaning. In skeletal representation, by pushing the resultant pose skeleton descriptor $s(y_{SPA})$ to target $s(y_{tar})$ to make the resultant skeleton similar to target. As the skeletal descriptor $s(\cdot)$ is differentiable, our network can effectively be updated to enforce the skeleton similarity during the model training process. Similar to $s(y_{SPA})$, $s(y_{tar})$ inherently comes from the target pose data y_{tar} . But as target pose data is not always available in practice, given $s(y_{tar})$ is low dimensional, we can tailor measure $s(y_{tar})$ directly from the exact target or other subjects from the same dataset.

The loss for SPA is given as:

$$L_{SPA} = \|f(y)\|_1 + \|s(y_{SPA}) - s(y_{tar})\|_2, \quad (4)$$

where, $s(y_{tar})$ stands for the target skeletal measures. We employ norm L_2 loss for skeletal similarity pivoting and use

norm L_1 loss for initial pose pivoting. In our design, SPA is trained after SAA, which acts as an additional component to the SAA network.

We have to point out that though human geometric has been employed for human pose estimation [68], it is given as an additional constraint in an end-to-end training process where the target 3D human pose is available. However, SPA can be added as a light weighted head on top of an existing pose estimation network for adaptation purpose and the training process is done without any target pose data and only with a series of low dimensional tailor measurements.

4 Performance Evaluation

To implement AHuP approach for monocular 3D human pose estimation, we configured the architecture in Fig. 1 by employing a ResNet [16] and an integral human pose head [56] for G and T networks, respectively. D is similar to [21] in its a feature-wise manner with kernel size 1.

4.1 AHuP Implementation Details

Our work is implemented via the PyTorch framework and each configuration is trained with a Nvidia v100 GPU. For the backbone feature extractor network G , although training from scratch converges, initialization from pre-trained weights via ImageNet can accelerate this process, so, our backbone network is initialized with the pre-trained weights from ImageNet [10]. All other networks are initialized via Xavier [13]. During training and test of SAA network (as introduced in main text Sec. 3.1), we chose batch size to be 120.

For feature-wise D shown in Fig. 1, we chose a 3-layer configuration. Networks G and T were jointly trained in an adversarial learning procedure with D playing as the counter part. Learning rate is set at $1e-3$ with a decreasing rate of 0.1 at epoch 11 and 13 with a total of 15. All input images are human centered, cropped and resized to be 256×256 . The output heatmap is set as $64 \times 64 \times 64$. During training, we initially train the 2D part at first 5 epochs to facilitate SAA process and 3D supervision is added after.

To facilitate the training and testing across different datasets, we choose the shared or similar joints to match the 17 joint configuration of the Human3.6M dataset by reordering and renaming. For data feeding, we followed a pivoted matching principle that whenever the leading feeder gives a batch, all subordinates will feed equivalent data to match. Since our study is focused on 3D human pose estimation, we always put the 3D pose dataset as the pivot feeder. For a fair comparison among varying size datasets, we fixed the iteration per epoch at 2500 by repeating the exhausted data loader, if any.

For SPA model, we decoupled it from the SAA net training process by learning the mapping directly from the ground truth data. To respect the convention to avoid using any information from the test data, we used the mean skeletal descriptor $s(y_{tar})$ of the training split with the assumption that it is similar to test split within the same dataset. We used a shallow 3 layer fully connected neural network for $f(y)$, where the first two layers are followed by a batch normalization and ReLU. The initial learning rate is set to be $1e-4$ with a decreasing rate of 0.95 at each epoch with a total 70 epoch and batch size 256. During the training, the SURREAL data is downsampled with the rate of 90 to become balanced with the ScanAva+ dataset. Human3.6M is also downsampled with the rate 5 for training and 64 for testing, as commonly done in related studies [39, 24, 66, 55, 56]. Our augmentation includes rotation, scaling, color jittering, and synthetic occlusion [67].

4.2 Evaluation Datasets

For AHuP performance evaluation and comparison with the SOTA, we employed several publicly-available datasets in the human pose estimation field that have been used extensively. For real 3D human pose data, we chose the Human3.6M [19] and MuPoTs [37] datasets to represent lab and outdoor environments respectively. For real 2D human pose data, we chose the MSCOCO [28] and MPII [2] datasets. As for synthetic human pose data, one branch comes from the deformable human template, in which we chose SURREAL dataset [61]. In SURREAL, we used the released train split to extract sample images. We kept a 0.05 portion of the whole section for validation and test purposes.

The other synthetic branch comes from the construction of virtual avatars through the direct 3D scanning of humans, in which we chose the ScanAva+ dataset developed in our lab [29]. The original ScanAva has only 15 scans which is fewer than its counterpart, SURREAL dataset. To balance the comparison in our study, we used the toolkit employed in the original ScanAva in order to collect additional human scans to augment the dataset to contain 41 full body scans and we formed the ScanAva+ dataset, in which 36 scans are used for the training. If not specifically indicated, we employed a basic setting with pose data from SYN + MPII + MSCOCO collectively for all synthetic union cases, where SYN stands for either ScanAva+ or SURREAL datasets.

4.3 Evaluation Metrics

To provide a comprehensive view in our evaluation, we employ extensively-used metrics from real human pose benchmarks to report our performance, including mean per joint

Table 1: Ablation study of AHuP when tested on real 3D human pose datasets as Human3.6M Protocol#2 and MuPoTs. C stands for a conventional adaptation from [9, 30, 54], SAA for semantic aware adaptation, Jo2D for adding 2D pose estimation tasks from additional 2D human pose dataset (MSCOCO and MPII datasets), SPA for adding skeletal pose adaptation.

Training Dataset + Adaptation Strategies	Human3.6M Protocol#2			MuPoTs		
	PA MPJPE	3DPCK	AUC	PA MPJPE	3DPCK	AUC
ScanAva+ [29]	180.3	29.3	20.3	240.8	32.9	11.9
ScanAva+ + C [9]	156.5	58.8	24.4	197.7	43.7	17.0
ScanAva+ + SAA	99.9	84.0	41.7	118.4	76.1	36.2
ScanAva+ + SAA + Jo2D	88.8	89.0	45.9	111.8	81.8	38.7
ScanAva + SAA + Jo2D + SPA	85.1	90.2	47.9	111.6	81.6	39.0
SURREAL [61]	181.4	44.9	16.4	187.0	42.7	15.3
SURREAL + C [9]	145.5	39.7	27.8	165.1	55.5	21.7
SURREAL + SAA	138.6	42.3	29.1	145.6	64.3	26.6
SURREAL + SAA + Jo2D	135.5	46.2	30.3	134.6	71.3	30.0
SURREAL + SAA + Jo2D + SPA	135.3	68.8	30.3	134.6	71.4	29.8

position error (MPJPE) for Human3.6M [19], 3D percentage of correct key-points (3DPCK), and the area under curve (AUC) for MuPoTs [37]. For MPJPE, we also reported the Procrustes analysis (PA MPJPE) version [14], which is more reliable and fair especially for cross-set evaluation due to varying camera parameters, joint definition, and body shape distributions.

For 3DPCK, we follow the official configuration of [37] with a 15cm tolerance for joint location estimation accuracy. We assume every human is correctly detected and compare all cases with pelvis rooted error. For Human3.6M, we also follow 2nd protocol during evaluation [66, 39], where subjects 9 and 11 are used for testing [4]. Due to the joint definition differences, we use Human3.6M as a template and map the similar joints and interpolate missing ones for other datasets. Please note that in the original protocols used in the majority of the 3D pose estimation works, the training split of the Human3.6M is employed during training, which we do not use at all. This makes our task a more challenging case (and at the same time more realistic in nature) than the original protocol.

4.4 Ablation Study

To evaluate how the proposed AHuP framework can enhance the 3D pose estimation with only 3D synthetic data, we added each component one by one to form the following settings: (1) pure 3D synthetic data based learning either with SURREAL or ScanAva+, (2) learning with conventional adaptation approach by aligning the whole feature space directly similar to [9, 30, 54], named with suffix 'C', (3) semantic aware adaptation with suffix 'SAA', (4) further adding 2D pose task from additional 2D human pose dataset (MSCOCO and MPII datasets) with suffix 'Jo2D', (5) further adding skeletal pose adaptation with suffix 'SPA'.

From the results shown in Tab. 1, we can see that conventional adaptation by aligning the whole features [59, 58] does improve the performance on both synthetic datasets

across all real benchmarks. By employing the SAA strategy, the improvement is significant on ScanAva+, and slightly but still noticeable on SURREAL. Additional 2D pose tasks from the real 2D human dataset shows further improvement which agrees with the existing studies [68]. SPA shows noticeable improvement for both ScanAva+ and SURREAL on Human3.6M but not much difference on MuPoTs. Although MuCo is the training split for MuPoTs [37], the two datasets are in fact captured in different environments separately, which could result in differences in the skeletal descriptors. We still notice that in the SURREAL case, although the improvement is not obvious on PA MPJPE, the 3DPCK metric is improved significantly. It shows that by adding SPA, many of the pose errors fall back into the tolerance range.

4.5 Qualitative Study in Pose and Feature Spaces

Tab. 1 shows that applying AHuP approach leads to pose estimation performance improvement on both real 3D pose benchmarks, however there are much stronger improvements when ScanAva+ dataset is used for training compared to the SURREAL. To figure out the underlying reason, we further investigated the characteristics of datasets themselves. We randomly extracted 5000 3D human pose samples from all four 3D datasets, including real (Human3.6M and MuPoTs) and synthetic (ScanAva+ and SURREAL) pose datasets, and visualized them via a t-distributed stochastic neighbor embedding (t-SNE) approach [33] in Fig. 3. This plot is purely based on the raw pelvis rooted 3D pose data without filtering after matching the joint order across datasets, in order to reflect the essential pose difference among these sets. From the plot, surprisingly we found out a higher agreement between all real datasets and ScanAva, yet a clear boundary around SURREAL. It seems SURREAL does not hold a well overlapping pose manifold with the others. The causes could be multi-fold, including the camera setting and joint definition in their render-

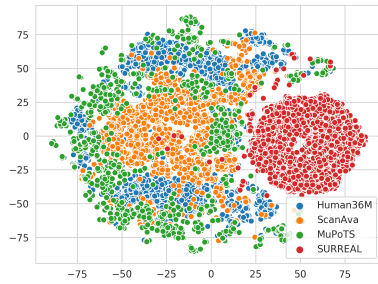


Fig. 3: t-SNE plot of pelvis rooted 3D pose data across 5000 data samples randomly extracted from Human3.6M, MuPoTS, ScanAva+ and SURREAL.

ing process, which all possibly affect the final pose distribution. When SURREAL is the only 3D source, the model can hardly learn any further than its pose coverage. This presumes to be the cause of limited improvements in the case when only SURREAL data is used.

It is also interesting to investigate how these approaches influence the feature space. To better illustrate this, we visualized the output features of G from all four datasets under different model configurations as shown in Fig. 4. Due to computational intensity and also to prevent a cluttered visualization, we evenly sampled 100 images from each dataset, with the G network’s output features downsampled to $1024 \times 4 \times 4$. Fig. 4 shows how differently each dataset is in the “eye” of these models. In Fig. 4a, all datasets show clear clustering effect. This is reasonable as the model based on only synthetic data can hardly generalize well to capture the shared features for both of real and synthetic data. With the adaptor introduction in Fig. 4b, the clustering effect has been eliminated much, but we notice that the synthetic features are more located on the right hand side for both SURREAL and ScanAva+. With SAA as shown in Fig. 4c, there is no obvious improvement over the C version, but the synthetic features are more evenly distributed in the space. With additional 2D task from real 2D human pose in Fig. 4d, the distribution becomes flattened. One interesting observation is that SURREAL shows a more obvious clustering effect than the adaptation only version. Instead of losing the generalization ability, we believe this clustering effect on the contrary indicates improved ability of the network to recognize different poses. As SURREAL does not hold a similar pose distribution to the others, it suppose to show a different pattern in a well recognized pose space.

4.6 Adaptation of SOTA Models using AHuP

Although our proposed AHuP approach shows improvement over the models trained on the synthetic human data, one immediate question is why bother to use AHuP given that well performed 3D human pose models already exist? Here,

we examine how AHuP is also capable to improve performance of the existing SOTA 3D pose estimation models when tested under a different context or dataset from their training set.

In order to conduct a fair comparison, we designed a cross-set evaluation experiment that all candidate models are trained and tested on different datasets to mimic the effect when they are employed in applications with novel contextx. We chose two SOTA pose estimation models introduced by Sun et al. in [56] and by Zhou et al. in [68] in this experimental analysis. To cover more possible scenarios, for top performer [56], we trained two networks with Human3.6M + MPII + MSCOCO and MuCo + MPII + MSCOCO, respectively. For [68], we employed their official release of the pre-trained model on Human3.6M + MPII. We tested both model on a 3D human pose dataset that was novel for them. As they already learned from the real domains with limited shift in the appearance, we only evaluated the effect of our SPA on these models. Their model performance with or without SPA is reported in Tab. 2. The results illustrate that adding AHuP adaptation in the form of SPA to these models leads to consistent performance improvement over the versions without SPA. These improvements are seen in both models [56,68] and in all of the training set combinations, and for different types of test sets.

4.7 Practical Values of AHuP

SPA can be employed as a switchable head on top of an existing network such as ResNet to act as a light weighted adaptation strategy. The adaptation can be achieved by simply switching the SPA head without retraining the network itself. The benefits of this SPA adaptation strategy includes:

- Time efficient adaptation: To evaluate a model on different benchmarks, it is common to train a specific model for each of the new benchmarks as suggested by [39]. However, retraining the model in [56] on a new dataset takes two days [39]. In contracts, training a SPA head takes less than 20 minutes.
- Memory efficient storage: Suppose we train a new model for each of the new dataset/context, the storage cost will be proportional to the number of the datasets scaled by the size of the network. However, in SPA adaptation, we only need one copy of the model (e.g. PoseNet) with different SPA adaptation heads. An example of the storage comparison for models in [56,68] with and without SPA strategy is shown in Fig. 5, where the more potential datasets to work on, the more memory saving our SPA adaptation will lead to.
- Efficient computational cost: Adding SPA in inference processes will inevitably increase the calculation cost, but the cost increase is actually negligible compared to

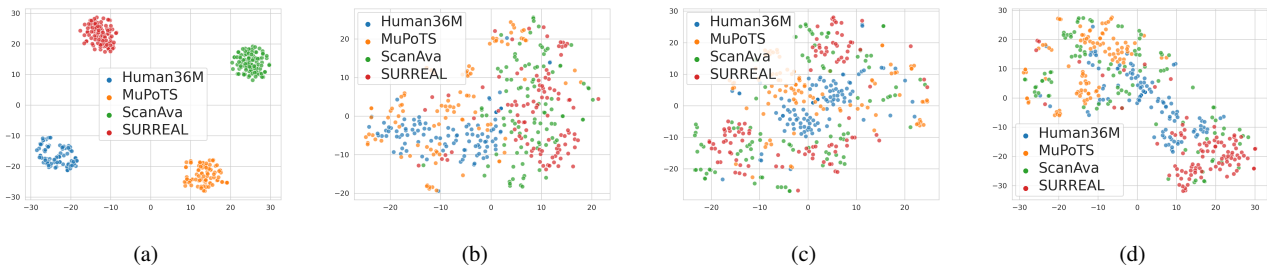


Fig. 4: t-SNE plot of network G 's output features applied on Human3.6M, MuPoTS, ScanAva+, and SURREAL datasets under model configurations of (a) no adaptation, (b) with a conventional adaptor C , (c) with SAA, (d) with SAA + Jo2D.

the computation of the original network. A comparison of computational cost of the two models in [56,68] is shown in Tab. 3.

4.8 Comparing 3D Pose Estimation Performance of AHuP with the SOTA

Fundamentally, our AHuP design focuses on performance improvement under a cross-set evaluation scenario. Nonetheless, to show AHuP performance in a larger picture,

Table 2: Cross benchmark evaluation of the 3D pose estimation models in [56] and [68], when trained and evaluated on different 3D pose datasets, with and without SPA. MuCo is the official training portion of the MuPoTS dataset [37].

Benchmarks	SPA	MPJPE PA	3DPCK	AUC
Sun et al. [56] trained on MuCo + MSCOCO + MPII				
Human36M	✗	82.1	75.8	49.0
	✓	77.9	92.7	51.5
ScanAva+	✗	92.6	87.7	43.7
	✓	91.7	87.7	44.2
SURREAL	✗	154.8	63.0	26.6
	✓	154.2	63.2	27.0
Sun et al. [56] trained on Human3.6M + MSCOCO + MPII				
MuPoTS	✗	111.1	84.1	41.0
	✓	105.9	84.1	41.1
ScanAva+	✗	111.8	77.5	38.1
	✓	106.9	79.2	40.8
SURREAL	✗	171.8	54.7	22.3
	✓	170.1	55.7	23.2
Zhou et al. [68] trained on Human3.6M + MPII				
MuPoTS	✗	111.8	77.5	38.1
	✓	106.9	79.2	40.8
ScanAva+	✗	91.6	87.5	44.0
	✓	89.1	87.8	45.5
SURREAL	✗	156.3	62.7	26.4
	✓	153.6	63.6	28.2

Table 3: Computational cost of the models in [56] and [68] with and without SPA in Giga flops.

Models	Original	+SPA	Computational cost increase (%)
Sun et al. [56]	13.097	13.101	0.031%
Zhou et al. [68]	12.003	12.007	0.033%

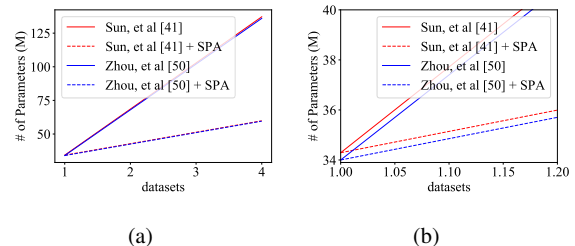


Fig. 5: Memory usage based on the number of parameters in million (M) in the SOTA models from [56] and [68], when customized for varying numbers of datasets with and without SPA: (a) in full scale, (b) zoomed in to show the slope differences.

we directly compare AHuP model performance trained on (ScanAva+ + MSCOCO + MPII) with the SOTA models on the reported metrics as shown in Tab. 4. Please note that this comparison is between AHuP without using any real 3D human pose data, and other models which directly benefit from using the training and test split from the same benchmarks [19,37], with no domain shift to overcome at all [56,66,39]. Following the convention in [39], we reported our performance under Human3.6M Protocol#2 as shown in Tab. 4. As 3D pose estimation is a scale-uncertain process, different datasets have different camera poses and parameters, which will directly affect the regression results. So, we also included the rigid Procrustes analysis (PA) alignment [14] result for a more just comparison. Though it cannot match the best performing models, we demonstrate that our model can already rival some approaches that learn directly from real 3D human pose data [66,7]. Furthermore, the difference in pose definition could introduce additional estimation errors. For example, in ScanAva+ the “head” joint lies at the top point of the head, yet in Human3.6M, this joint is biased towards the head center. The “ankle joint” in Human 3.6M lies at the back of the heel, yet ScanAva+ and SURREAL place them closer to the center of the ankle above the foot.

One question is whether or not we really benefit from the learned features that extracted from the synthetic data

Table 4: Comparison with the state-of-the-art based on the MPJPE metric tested on Human3.6M dataset using Protocol#2. Please note that unlike AHuP, all of these models have used some real 3D human pose data in their training process. For our method, PA stands for when the PA rigid alignment is applied. The last two rows stands for Martinez approach [35] trained on ScanAva+ dataset.

Methods	Dir	Dis	Eat	Gre	Phon.	Pose	Pur.	Sit	SitD	Smo.	Phot.	Wait	Walk	WalkD.	WalkP.	Avg
Akhter & Black [1]	199.2	177.6	161.8	197.8	176.2	186.5	195.4	167.3	160.7	173.7	177.8	181.9	176.2	198.6	192.7	181.1
Ramakrishna [49]	137.4	149.3	141.6	154.3	157.7	158.9	141.8	158.1	168.6	175.6	160.4	161.7	150.0	174.8	150.2	157.3
Zhou [70]	99.7	95.8	87.9	116.8	108.3	107.3	93.5	95.3	109.1	137.5	106.0	102.2	106.5	110.4	115.2	106.7
SMPLify [4]	62.0	60.2	67.8	76.5	92.1	77.0	73.0	75.3	100.3	137.3	83.4	77.3	79.7	86.8	81.7	82.3
Chen[7]	89.9	97.6	90.0	107.9	107.3	93.6	136.1	133.1	240.1	106.7	139.2	106.2	87.0	114.1	90.6	114.2
Tome [57]	65.0	73.5	76.8	86.4	86.3	68.9	74.8	110.2	173.9	85.0	110.7	85.8	71.4	86.3	73.1	88.4
Moreno [40]	69.5	80.2	78.2	87.0	100.8	76.0	69.7	104.7	113.9	89.7	102.7	98.5	79.2	82.4	77.2	87.3
Zhou [71]	68.7	74.8	67.8	76.4	76.3	84.0	70.2	88.0	113.8	78.0	98.4	90.1	62.6	75.1	73.6	79.9
Jahangiri [22]	74.4	66.7	67.9	75.2	77.3	70.6	64.5	95.6	127.3	79.6	79.1	73.4	67.4	71.8	72.8	77.6
Mehta [36]	57.5	68.6	59.6	67.3	78.1	56.9	69.1	98.0	117.5	69.5	82.4	68.0	55.3	76.5	61.4	72.9
Martinez [35]	51.8	56.2	58.1	59.0	69.5	55.2	58.1	74.0	94.6	62.3	78.4	59.1	49.5	65.1	52.4	62.9
Fang [11]	50.1	54.3	57.0	57.1	66.6	53.4	55.7	72.8	88.6	60.3	73.3	57.7	47.5	62.7	50.6	60.4
Sun [55]	52.8	54.8	54.2	54.3	61.8	53.1	53.6	71.7	86.7	61.5	67.2	53.4	47.1	61.6	63.4	59.1
Sun [11]	47.5	47.7	49.5	50.2	51.4	43.8	46.4	58.9	65.7	49.4	55.8	47.8	38.9	49.0	43.8	49.6
Moon [39]	50.5	55.7	50.1	51.7	53.9	46.8	50.0	61.9	68.0	52.5	55.9	49.9	41.8	56.1	46.9	53.3
ScanAva-AHuP	135.9	137.2	104.0	137.1	139.4	133.6	140.8	133.7	163.3	129.5	137.9	139.5	123.2	135.1	130.2	134.5
ScanAva-AHuP PA	75.2	79.1	68.0	79.1	91.7	75.8	82.3	100.9	128.0	87.4	83.3	81.8	76.8	82.2	78.3	85.1
Martinez (ScanAva+) [35]	153.2	152.6	129.7	153.8	151.9	149.9	144.0	159.8	191.0	146.2	147.9	158.7	148.5	140.8	139.8	151.5
Martinez (ScanAva+) [35] PA	97.8	97.9	93.1	99.5	105.7	91.3	91.0	121.4	139.7	104.6	96.6	99.5	105.2	98.2	98.0	103.3

Table 5: 3DPCK comparison with the state-of-the-art tested on the MuPoTS dataset. 16 out of 20 subjects are listed due to space limitation.

Methods	S1	S2	S3	S4	S5	S6	S7	S8	S9	S10	S11	S12	S13	S14	S15	S16	...	Avg	AUC
Rogez [51]	67.7	49.8	53.4	59.1	67.5	22.8	43.7	49.9	31.1	78.1	50.2	51.0	51.6	49.3	56.2	66.5	...	53.8	27.6
Mehta [38]	81.0	60.9	64.4	63.0	69.1	30.3	65.0	59.6	64.1	83.9	68.0	68.6	62.3	59.2	70.1	80.0	...	66.0	37.8
Rogez [52]	87.3	61.9	67.9	74.6	78.8	48.9	58.3	59.7	78.1	89.5	69.2	73.8	66.2	56.0	74.1	82.1	...	70.6	-
Moon [39]	94.4	77.5	79.0	81.9	85.3	72.8	81.9	75.7	90.2	90.4	79.2	79.9	75.1	72.7	81.1	89.9	...	81.8	-
ScanAva-AHuP	90.6	75.0	66.0	73.5	87.6	73.5	90.7	71.1	91.0	95.0	87.1	87.6	74.2	68.6	85.9	72.0	...	81.6	39.0

with the SAA or it is just a 2D-to-3D lifting. To investigate this question, we specifically trained a 2D-to-3D lifting SOTA model [35] under the same setting of AHuP with synthetic ScanAva+ data. Its performance is reported as Martinez (ScanAva+) in the Tab. 4, which shows that AHuP still performs noticeably better than 2D-to-3D lifting version when employed under the same setting.

Another set of real 3D pose data evaluation is conducted on MuPoTS [37] with results shown in Tab. 5. It is quite surprising that despite the fact that we do not use a single frame of real 3D human data, AHuP shows competitive performance among SOTA models that are trained on the real 3D human pose data. This mainly stems from the fact that MuPoTS is collected in the wild with multiple people, so the images are in a more natural setting. In comparison, Human3.6M is collected in a studio environment with limited number of subjects. For a fixed lab setting such as Human3.6M, many context factors such as camera pose and background can inherently be well studied from its corresponding training set, but it is not the case for MuPoTS, since its data seems to have higher variations in these factors.

4.9 Qualitative Comparison

We also visualized the recovered 3D pose results when AHuP trained on ScanAva+ is used (see Fig. 6). Despite

the lower performance compared to the top rank 3D pose estimation models, the recovered skeletons via our method agree well with human perception. In fact, when recovered joints are within a tolerable error threshold, from a human perspective, our prediction is “semantically” correct. We also tested AHuP on synthetic data in the last two columns of Fig. 6, which performs equivalently well.

4.10 Evaluation in 3D Multi-Person Pose Estimation

Our approach also shows compatibility with other works. Combining with the proposed approach in [39] by employing Mask-RCNN [15] as detect-net (for human detection), our model can be well integrated as a pose-net (for 3D human pose estimation) for multi-person pose estimation. As multi-person performance is also affected by root localization, we only report qualitative result as shown in Fig. 7 without taking credits from [39].

5 Conclusion

The ultimate goal of training an inference model is to make the model ready to perform in some real world applications. Training and testing under different contexts potentially introduces the domain gap and influences the model performance negatively. This issue is especially magnified in the

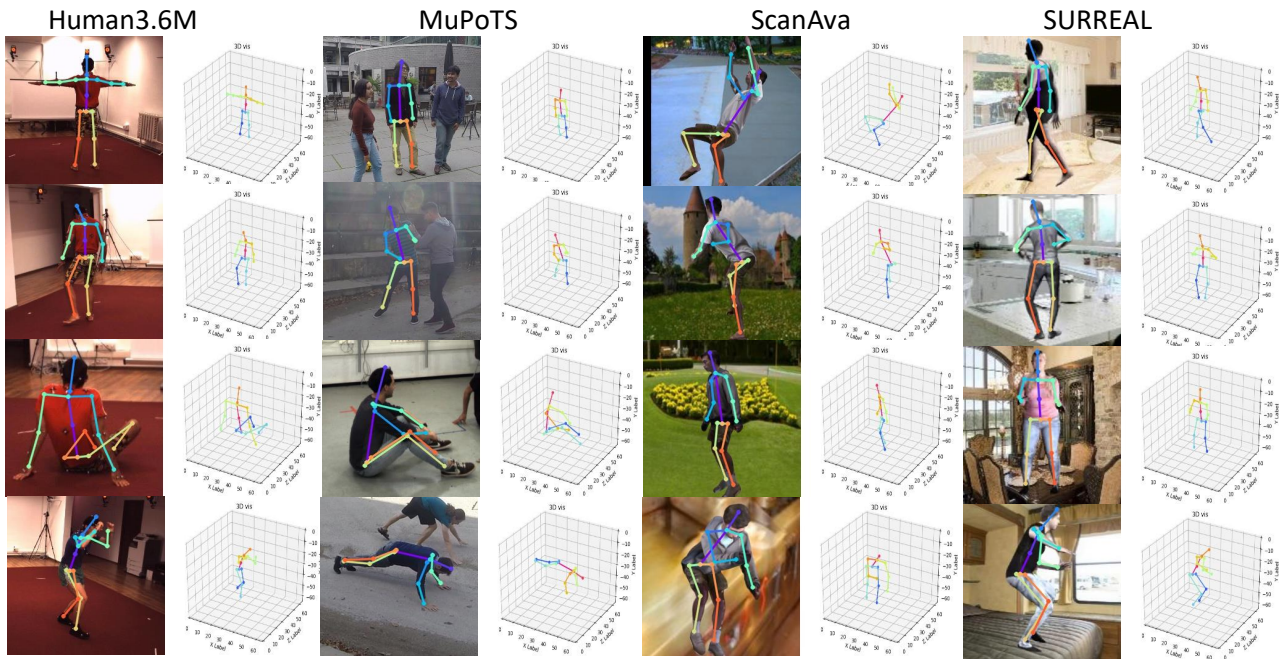


Fig. 6: Qualitative recovery results of AHuP trained on ScanAva+ tested across domains and datasets.

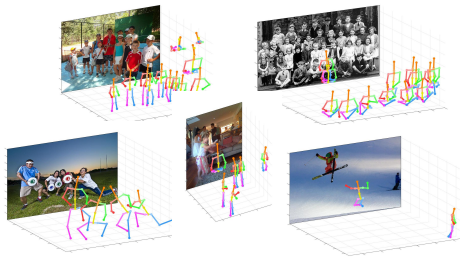


Fig. 7: Qualitative recovery results of ScanAva-AHuP on MSCOCO dataset.

3D human pose problem, where the majority of the 3D human pose benchmarks are collected under controlled lab settings. To mitigate this effect, we presented our adapted human pose (AHuP) approach that incorporates a semantic awareness adaptation (SAA) technique as well as a skeletal pose adaptation (SPA) algorithm and illustrated how AHuP improves 3D pose estimation model performance both quantitatively and qualitatively. For a better illustration of an application with a significant context shift, we chose the synthetic human data to train our inference model on without using any real 3D human pose data. We then tested AHuP on the well known 3D human pose benchmarks, in which it showed comparable performance with many of the state-of-the-art (SOTA) models, which have full access to the real 3D pose data. For existing SOTA models, our approach can also be added as a light weighted adaptation head which showed consistent improvement for all the candidate models, over

all training and testing combinations in our study. Admittedly, without having access to the target real 3D human data, AHuP has challenge to beat the best performers. However, in a real life problem, the solution we care most about is often not what we can achieve under an ideal condition (such as a controlled lab setting). Instead, it is practical to assume that the data from target domain is unavailable or we only have limited access to them. This is the foundation behind introducing AHuP.

References

1. Akhter, I., Black, M.J.: Pose-conditioned joint angle limits for 3d human pose reconstruction. In: Proceedings of the IEEE conference on computer vision and pattern recognition, pp. 1446–1455 (2015) [10](#)
2. Andriluka, M., Pishchulin, L., Gehler, P., Schiele, B.: 2d human pose estimation: New benchmark and state of the art analysis. In: Proceedings of the IEEE Conference on computer Vision and Pattern Recognition, pp. 3686–3693 (2014) [6](#)
3. Anguelov, D., Srinivasan, P., Koller, D., Thrun, S., Rodgers, J., Davis, J.: Scape: shape completion and animation of people. In: ACM transactions on graphics (TOG), vol. 24, pp. 408–416. ACM (2005) [3](#)
4. Bogo, F., Kanazawa, A., Lassner, C., Gehler, P., Romero, J., Black, M.J.: Keep it smpl: Automatic estimation of 3d human pose and shape from a single image. In: European Conference on Computer Vision, pp. 561–578. Springer (2016) [2](#), [3](#), [5](#), [7](#), [10](#)
5. Butler, D.J., Wulff, J., Stanley, G.B., Black, M.J.: A naturalistic open source movie for optical flow evaluation. In: European conference on computer vision, pp. 611–625. Springer (2012) [3](#)
6. Cao, M., Zhou, X., Xu, Y., Pang, Y., Yao, B.: Adversarial domain adaptation with semantic consistency for cross-domain im-

- age classification. In: Proceedings of the 28th ACM International Conference on Information and Knowledge Management, CIKM '19, p. 259–268. Association for Computing Machinery, New York, NY, USA (2019). DOI 10.1145/3357384.3357918. URL <https://doi-org.ezproxy.neu.edu/10.1145/3357384.3357918> 3
7. Chen, C.H., Ramanan, D.: 3d human pose estimation= 2d pose estimation+ matching. In: Proceedings of the IEEE Conference on Computer Vision and Pattern Recognition, pp. 7035–7043 (2017) 9, 10
 8. Chen, C.H., Tyagi, A., Agrawal, A., Drover, D., Stojanov, S., Rehg, J.M.: Unsupervised 3d pose estimation with geometric self-supervision. In: Proceedings of the IEEE Conference on Computer Vision and Pattern Recognition, pp. 5714–5724 (2019) 1, 2, 3, 5
 9. Chen, W., Wang, H., Li, Y., Su, H., Wang, Z., Tu, C., Lischinski, D., Cohen-Or, D., Chen, B.: Synthesizing training images for boosting human 3d pose estimation. In: 2016 Fourth International Conference on 3D Vision (3DV), pp. 479–488. IEEE (2016) 3, 7
 10. Deng, J., Dong, W., Socher, R., Li, L.J., Li, K., Fei-Fei, L.: Imagenet: A large-scale hierarchical image database. In: 2009 IEEE conference on computer vision and pattern recognition, pp. 248–255. Ieee (2009) 6
 11. Fang, H.S., Xu, Y., Wang, W., Liu, X., Zhu, S.C.: Learning pose grammar to encode human body configuration for 3d pose estimation. In: Thirty-Second AAAI Conference on Artificial Intelligence (2018) 10
 12. Ganin, Y., Ustinova, E., Ajakan, H., Germain, P., Larochelle, H., Laviolette, F., Marchand, M., Lempitsky, V.: Domain-adversarial training of neural networks. *The Journal of Machine Learning Research* 17(1), 2096–2030 (2016) 1, 3
 13. Glorot, X., Bengio, Y.: Understanding the difficulty of training deep feedforward neural networks. In: Proceedings of the thirteenth international conference on artificial intelligence and statistics, pp. 249–256 (2010) 6
 14. Gower, J.C.: Generalized procrustes analysis. *Psychometrika* 40(1), 33–51 (1975) 7, 9
 15. He, K., Gkioxari, G., Dollár, P., Girshick, R.: Mask r-cnn. In: Proceedings of the IEEE international conference on computer vision, pp. 2961–2969 (2017) 10
 16. He, K., Zhang, X., Ren, S., Sun, J.: Deep residual learning for image recognition. In: Proceedings of the IEEE conference on computer vision and pattern recognition, pp. 770–778 (2016) 6
 17. Hoffman, J., Tzeng, E., Park, T., Zhu, J.Y., Isola, P., Saenko, K., Efros, A., Darrell, T.: Cycada: Cycle-consistent adversarial domain adaptation. In: Proceedings of the 35th International Conference on Machine Learning (2018) 3, 4
 18. Hong, Z.W., Yu-Ming, C., Su, S.Y., Shann, T.Y., Chang, Y.H., Yang, H.K., Ho, B.H.L., Tu, C.C., Chang, Y.C., Hsiao, T.C., et al.: Virtual-to-real: Learning to control in visual semantic segmentation. arXiv preprint arXiv:1802.00285 (2018) 3
 19. Ionescu, C., Papava, D., Olaru, V., Sminchisescu, C.: Human3.6m: Large scale datasets and predictive methods for 3d human sensing in natural environments. *IEEE Transactions on Pattern Analysis and Machine Intelligence* 36(7), 1325–1339 (2014) 1, 3, 6, 7, 9
 20. Iqbal, U., Molchanov, P., Kautz, J.: Weakly-supervised 3d human pose learning via multi-view images in the wild. In: Proceedings of the IEEE/CVF Conference on Computer Vision and Pattern Recognition (CVPR) (2020) 3
 21. Isola, P., Zhu, J.Y., Zhou, T., Efros, A.A.: Image-to-image translation with conditional adversarial networks. In: Computer Vision and Pattern Recognition (CVPR), 2017 IEEE Conference on (2017) 3, 4, 5, 6
 22. Jahangiri, E., Yuille, A.L.: Generating multiple diverse hypotheses for human 3d pose consistent with 2d joint detections. In: Proceedings of the IEEE International Conference on Computer Vision, pp. 805–814 (2017) 10
 23. Kocabas, M., Karagoz, S., Akbas, E.: Self-supervised learning of 3d human pose using multi-view geometry. arXiv preprint arXiv:1903.02330 (2019) 3
 24. Lassner, C., Romero, J., Kiefel, M., Bogo, F., Black, M.J., Gehler, P.V.: Unite the people: Closing the loop between 3d and 2d human representations. In: Proceedings of the IEEE Conference on Computer Vision and Pattern Recognition, pp. 6050–6059 (2017) 6
 25. Li, S., Chan, A.B.: 3d human pose estimation from monocular images with deep convolutional neural network. In: Asian Conference on Computer Vision, pp. 332–347. Springer (2014) 1
 26. Li, S., Ke, L., Pratama, K., Tai, Y.W., Tang, C.K., Cheng, K.T.: Cascaded deep monocular 3d human pose estimation with evolutionary training data. In: Proceedings of the IEEE/CVF Conference on Computer Vision and Pattern Recognition (CVPR) (2020) 2
 27. Liebelt, J., Schmid, C.: Multi-view object class detection with a 3d geometric model. In: 2010 IEEE Computer Society Conference on Computer Vision and Pattern Recognition, pp. 1688–1695. IEEE (2010) 3
 28. Lin, T.Y., Maire, M., Belongie, S., Hays, J., Perona, P., Ramanan, D., Dollár, P., Zitnick, C.L.: Microsoft coco: Common objects in context. In: European conference on computer vision, pp. 740–755. Springer (2014) 6
 29. Liu, S., Ostadabbas, S.: A semi-supervised data augmentation approach using 3d graphical engines. In: Proceedings of the European Conference on Computer Vision (ECCV), pp. 0–0 (2018) 3, 6, 7
 30. Long, M., Cao, Y., Wang, J., Jordan, M.I.: Learning transferable features with deep adaptation networks. arXiv preprint arXiv:1502.02791 (2015) 3, 7
 31. Loper, M., Mahmood, N., Black, M.J.: Mosh: Motion and shape capture from sparse markers. *ACM Transactions on Graphics (TOG)* 33(6), 1–13 (2014) 2
 32. Luo, Y., Zheng, L., Guan, T., Yu, J., Yang, Y.: Taking a closer look at domain shift: Category-level adversaries for semantics consistent domain adaptation. In: Proceedings of the IEEE/CVF Conference on Computer Vision and Pattern Recognition (CVPR) (2019) 3, 4
 33. Maaten, L.v.d., Hinton, G.: Visualizing data using t-sne. *Journal of machine learning research* 9(Nov), 2579–2605 (2008) 7
 34. Marin, J., Vázquez, D., Gerónimo, D., López, A.M.: Learning appearance in virtual scenarios for pedestrian detection. In: 2010 IEEE computer society conference on computer vision and pattern recognition, pp. 137–144. IEEE (2010) 3
 35. Martinez, J., Hossain, R., Romero, J., Little, J.J.: A simple yet effective baseline for 3d human pose estimation. In: Proceedings of the IEEE International Conference on Computer Vision, pp. 2640–2649 (2017) 1, 2, 10
 36. Mehta, D., Rhodin, H., Casas, D., Fua, P., Sotnychenko, O., Xu, W., Theobalt, C.: Monocular 3d human pose estimation in the wild using improved cnn supervision. In: 2017 International Conference on 3D Vision (3DV), pp. 506–516 (2017) 10
 37. Mehta, D., Sotnychenko, O., Mueller, F., Xu, W., Sridhar, S., Pons-Moll, G., Theobalt, C.: Single-shot multi-person 3d pose estimation from monocular rgb. In: 3D Vision (3DV), 2018 Sixth International Conference on. IEEE (2018). URL <http://gvv.mpi-inf.mpg.de/projects/SingleShotMultiPerson> 1, 6, 7, 9, 10
 38. Mehta, D., Sotnychenko, O., Mueller, F., Xu, W., Sridhar, S., Pons-Moll, G., Theobalt, C.: Single-shot multi-person 3d pose estimation from monocular rgb. In: 2018 International Conference on 3D Vision (3DV), pp. 120–130. IEEE (2018) 10
 39. Moon, G., Chang, J.Y., Lee, K.M.: Camera distance-aware top-down approach for 3d multi-person pose estimation from a single rgb image. In: Proceedings of the IEEE International Conference on Computer Vision, pp. 10133–10142 (2019) 4, 6, 7, 8, 9, 10

40. Moreno-Noguer, F.: 3d human pose estimation from a single image via distance matrix regression. In: Proceedings of the IEEE Conference on Computer Vision and Pattern Recognition, pp. 2823–2832 (2017) [10](#)
41. Morgado, P., Vasconcelos, N.: Semantically consistent regularization for zero-shot recognition. In: Proceedings of the IEEE Conference on Computer Vision and Pattern Recognition (CVPR) (2017) [4](#)
42. Newell, A., Yang, K., Deng, J.: Stacked hourglass networks for human pose estimation. European Conference on Computer Vision pp. 483–499 (2016) [3](#)
43. Pavlo, D., Feichtenhofer, C., Grangier, D., Auli, M.: 3d human pose estimation in video with temporal convolutions and semi-supervised training. In: Conference on Computer Vision and Pattern Recognition (CVPR) (2019) [3](#)
44. Peng, X., Sun, B., Ali, K., Saenko, K.: Learning deep object detectors from 3d models. In: Proceedings of the IEEE International Conference on Computer Vision, pp. 1278–1286 (2015) [3](#)
45. Peris, M., Martull, S., Maki, A., Ohkawa, Y., Fukui, K.: Towards a simulation driven stereo vision system. In: Proceedings of the 21st International Conference on Pattern Recognition (ICPR2012), pp. 1038–1042. IEEE (2012) [3](#)
46. Popa, A.I., Zanfir, M., Sminchisescu, C.: Deep multitask architecture for integrated 2d and 3d human sensing. In: Proceedings of the IEEE Conference on Computer Vision and Pattern Recognition, pp. 6289–6298 (2017) [3](#)
47. Quiñero-Candela, J., Sugiyama, M., Schwaighofer, A., Lawrence, N.: Covariate shift and local learning by distribution matching (2008) [4](#)
48. Ragheb, H., Velastin, S., Remagnino, P., Ellis, T.: Vihasi: virtual human action silhouette data for the performance evaluation of silhouette-based action recognition methods. In: 2008 Second ACM/IEEE International Conference on Distributed Smart Cameras, pp. 1–10. IEEE (2008) [3](#)
49. Ramakrishna, V., Kanade, T., Sheikh, Y.: Reconstructing 3d human pose from 2d image landmarks. In: European Conference on Computer Vision, pp. 573–586. Springer (2012) [10](#)
50. Remelli, E., Han, S., Honari, S., Fua, P., Wang, R.: Lightweight multi-view 3d pose estimation through camera-disentangled representation. In: IEEE/CVF Conference on Computer Vision and Pattern Recognition (CVPR) (2020) [3](#)
51. Rogez, G., Weinzaepfel, P., Schmid, C.: Lcr-net: Localization-classification-regression for human pose. In: Proceedings of the IEEE Conference on Computer Vision and Pattern Recognition, pp. 3433–3441 (2017) [10](#)
52. Rogez, G., Weinzaepfel, P., Schmid, C.: Lcr-net++: Multi-person 2d and 3d pose detection in natural images. IEEE transactions on pattern analysis and machine intelligence (2019) [10](#)
53. Sigal, L., Balan, A.O., Black, M.J.: Humaneva: Synchronized video and motion capture dataset and baseline algorithm for evaluation of articulated human motion. International journal of computer vision **87**(1-2), 4 (2010) [3](#)
54. Sun, B., Saenko, K.: Deep coral: Correlation alignment for deep domain adaptation. In: European Conference on Computer Vision, pp. 443–450. Springer (2016) [3](#), [5](#), [7](#)
55. Sun, X., Shang, J., Liang, S., Wei, Y.: Compositional human pose regression. In: Proceedings of the IEEE International Conference on Computer Vision, pp. 2602–2611 (2017) [6](#), [10](#)
56. Sun, X., Xiao, B., Wei, F., Liang, S., Wei, Y.: Integral human pose regression. In: Proceedings of the European Conference on Computer Vision (ECCV), pp. 529–545 (2018) [6](#), [8](#), [9](#)
57. Tome, D., Russell, C., Agapito, L.: Lifting from the deep: Convolutional 3d pose estimation from a single image. In: Proceedings of the IEEE Conference on Computer Vision and Pattern Recognition, pp. 2500–2509 (2017) [10](#)
58. Tzeng, E., Hoffman, J., Darrell, T., Saenko, K.: Simultaneous deep transfer across domains and tasks. In: Proceedings of the IEEE International Conference on Computer Vision, pp. 4068–4076 (2015) [1](#), [3](#), [4](#), [5](#), [7](#)
59. Tzeng, E., Hoffman, J., Saenko, K., Darrell, T.: Adversarial discriminative domain adaptation. In: Proceedings of the IEEE Conference on Computer Vision and Pattern Recognition, pp. 7167–7176 (2017) [4](#), [5](#), [7](#)
60. Tzeng, E., Hoffman, J., Zhang, N., Saenko, K., Darrell, T.: Deep domain confusion: Maximizing for domain invariance. arXiv preprint arXiv:1412.3474 (2014) [3](#)
61. Varol, G., Romero, J., Martin, X., Mahmood, N., Black, M.J., Laptev, I., Schmid, C.: Learning from synthetic humans. In: CVPR (2017) [2](#), [3](#), [6](#), [7](#)
62. Wang, M., Yang, G.Y., Li, R., Liang, R.Z., Zhang, S.H., Hall, P.M., Hu, S.M.: Example-guided style-consistent image synthesis from semantic labeling. In: Proceedings of the IEEE/CVF Conference on Computer Vision and Pattern Recognition (CVPR) (2019) [3](#), [4](#)
63. Wang, Q., Gao, J., Lin, W., Yuan, Y.: Learning from synthetic data for crowd counting in the wild. In: Proceedings of the IEEE Conference on Computer Vision and Pattern Recognition, pp. 8198–8207 (2019) [3](#)
64. Xu, J., Yu, Z., Ni, B., Yang, J., Yang, X., Zhang, W.: Deep kinematics analysis for monocular 3d human pose estimation. In: Proceedings of the IEEE/CVF Conference on Computer Vision and Pattern Recognition (CVPR) (2020) [3](#)
65. Yang, W., Ouyang, W., Wang, X., Ren, J., Li, H., Wang, X.: 3d human pose estimation in the wild by adversarial learning. In: Proceedings of the IEEE Conference on Computer Vision and Pattern Recognition, pp. 5255–5264 (2018) [4](#), [5](#)
66. Yasin, H., Iqbal, U., Kruger, B., Weber, A., Gall, J.: A dual-source approach for 3d pose estimation from a single image. In: Proceedings of the IEEE Conference on Computer Vision and Pattern Recognition, pp. 4948–4956 (2016) [6](#), [7](#), [9](#)
67. Zhong, Z., Zheng, L., Kang, G., Li, S., Yang, Y.: Random erasing data augmentation. arXiv preprint arXiv:1708.04896 (2017) [6](#)
68. Zhou, X., Huang, Q., Sun, X., Xue, X., Wei, Y.: Towards 3d human pose estimation in the wild: a weakly-supervised approach. In: Proceedings of the IEEE International Conference on Computer Vision, pp. 398–407 (2017) [3](#), [4](#), [6](#), [7](#), [8](#), [9](#)
69. Zhou, X., Leonardos, S., Hu, X., Daniilidis, K.: 3d shape estimation from 2d landmarks: A convex relaxation approach. In: proceedings of the IEEE conference on computer vision and pattern recognition, pp. 4447–4455 (2015) [3](#)
70. Zhou, X., Zhu, M., Leonardos, S., Daniilidis, K.: Sparse representation for 3d shape estimation: A convex relaxation approach. IEEE transactions on pattern analysis and machine intelligence **39**(8), 1648–1661 (2016) [10](#)
71. Zhou, X., Zhu, M., Pavlakos, G., Leonardos, S., Derpanis, K.G., Daniilidis, K.: Monocap: Monocular human motion capture using a cnn coupled with a geometric prior. IEEE transactions on pattern analysis and machine intelligence **41**(4), 901–914 (2018) [10](#)
72. Zhu, J.Y., Park, T., Isola, P., Efros, A.A.: Unpaired image-to-image translation using cycle-consistent adversarial networks. In: Proceedings of the IEEE international conference on computer vision, pp. 2223–2232 (2017) [3](#)